Quaternion-Based Hybrid Feedback for Robust Global Attitude Synchronization*

Christopher G. Mayhew[♯], Ricardo G. Sanfelice[‡], Jansen Sheng[♭], Murat Arcak[♭], and Andrew R. Teel[†]

***Abstract*—We apply recent results on robust global asymptotic stabilization of the attitude of a single rigid body to the problem of globally synchronizing the attitude of a network of rigid bodies using a decentralized strategy. The proposed hybrid feedback scheme relies on the communication of a binary logic variable between each pair of neighboring rigid bodies that determines the orientation of a torque component acting to reduce their relative error. Through a hysteretic switch of this logic variable, the hybrid feedback achieves global synchronization under the assumption that the network is connected and acyclic. The hysteresis eliminates chattering while preventing the "unwinding phenomenon" apparent in some quaternion-based attitude control schemes. The results are exercised in a numerical example.**

I. Introduction

The problem of attitude synchronization among multiple rigid bodies has received attention in the recent literature [1]–[8] due to the promise of multiple spacecraft missions in deep space exploration [9], [10]. Although a number of attitude synchronization schemes have been presented, these designs are either non-global, subject to the "unwinding phenomenon" described below, or are not robust to measurement noise. These issues stem from the underlying state space of rigid body attitude, $\mathsf{SO}(3)$, whose topological complexities preclude the existence of smooth globally stabilizing feedbacks [11].

When smooth state-feedback is applied to stabilize the attitude of a rigid body, the best achievable result is *almost* global asymptotic stability, where the basin of attraction for a desired attitude excludes only a nowhere dense set of measure zero. Such results have been achieved, for example, in [12]. These topological problems directly affect the problem of attitude synchronization. We note that feedbacks for attitude synchronization that are similar to [12] appear in [7], where only local results are claimed, although the authors of [7] noted a "large" basin of attraction in simulations.

The topological complexity of $\mathsf{SO}(3)$ further affects control laws based on parameterizations of $\mathsf{SO}(3)$. In fact, every three-parameter parametrization of $\mathsf{SO}(3)$ is not globally nonsingular [13], which hinders their use for global synchronization of rigid-body attitude. Often, unit quaternions are used to parametrize $\mathsf{SO}(3)$ by means of a two-to-one covering map. When this parametrization is used, it creates the need to stabilize a two-point set of in the quaternion space [14]. Quaternion-based attitude control laws often neglect this double covering, sometimes resulting in an undesirable symptom termed *the unwinding phenomenon* [11] where the control law may unnecessarily rotate the body through a full rotation. Quaternion-based control schemes that induce this behavior may achieve a global synchronization result (i.e. convergence to a synchronized state); however, this synchronized state can be stable, or unstable, depending on the controller's quaternion representation of attitude [11], [14].

Unwinding can be avoided by a judicious selection of control law. For example, [5] proposes a synchronization scheme that causes unwinding, then reveals how to modify the proposed feedback in a smooth fashion to avoid this problem. The resulting feedback is closely related to the feedbacks used in [7], which achieve almost global asymptotic stability of the synchronized state. Other results, such as those in [8], use a memoryless quaternion-based feedback that is discontinuous at attitudes of 180°. Such a feedback avoids unwinding and results in global asymptotic stability of the desired synchronization, but it is not robust to arbitrarily small measurement disturbances [15].

In this paper, we propose a hybrid feedback that achieves rigid-body synchronization in connected and acyclic networks from any initial condition. The strategy enjoys robustness to measurement disturbances and also avoids the unwinding phenomenon. Here, we apply the main ideas of [15] to the quaternion-based attitude synchronization scheme in [3]. The enabling mechanism for our results is a logic variable associated with each relative attitude error that determines the sign of a potential-based torque component. The logic variable is updated hysteretically in a way that manages a trade-off between robustness to measurement disturbances and the "amount" of unwinding. Thus, the proposed scheme necessitates the communication of this logic variable between neighboring rigid bodies.

Finally, we remark that whether or not unwinding occurs, whether one should avoid the 180° rotation, and the correctness of many stability and convergence results, including the results in this paper, largely depend on *how* one maintains the quaternion parameterization of attitude. We refer the reader to the recent study [14], where it is shown that a simple (hybrid) dynamic mechanism can smoothly lift attitude measure-

[♯]mayhew@ieee.org, Robert Bosch Research and Technology Center, 4005 Miranda Ave., Palo Alto, CA 94304.

[‡]sricardo@u.arizona.edu, Department of Aerospace and Mechanical Engineering, University of Arizona, Tucson, AZ 85721.

[†]teel@ece.ucsb.edu, Center for Control Engineering and Computation, Electrical and Computer Engineering Department, University of California, Santa Barbara, CA 93106-9560.

[♭]{arcak,jsheng87}@eecs.berkeley.edu, Electrical Engineering and Computer Sciences, University of California, Berkeley, CA 94720.

*Research partially supported by the National Science Foundation under grant ECCS-0925637, grant CNS-0720842, grant ECCS-0852750 and by the Air Force Office of Scientific Research under grant FA9550-09-1-0203 and grant FA9550-09-1-0092.

ments onto the unit-quaternion space and seamlessly translate quaternion-based feedback controllers with their asymptotic stability properties to the actual rigid-body state space extended by an extra quaternion memory state. As in related literature, we assume that this mechanism is working in the background and omit it from the analysis.

The remainder of the paper is organized as follows. Section II discusses our multi-agent framework borrowed from [3], [16], attitude representation by unit quaternions, attitude kinematics and dynamics, relative error coordinates, and our hybrid system framework borrowed from [17]. Section III introduces the decentralized hybrid synchronization scheme and proves the robust global synchronization result, which is illustrated by simulation in Section IV. Finally, we make some concluding remarks in Section V.

II. Preliminaries

A. Multi-agent framework

Following [3], [16], we consider a network of N rigid bodies (agents), whose inter-agent information flow is represented by a graph. When two rigid bodies in the network have access to relative attitude information and can communicate a single binary logic variable, we let them be connected by a link of the graph. For each link connecting two agents, we arbitrarily assign an index, a positive end, and a negative end. Let M denote the total number of graph links, let $\mathcal{N} = \{1, \dots, N\}$ denote the set of agents, and let $\mathcal{M} = \{1, \dots, M\}$ denote the set of graph links. We define $\mathcal{M}_i^+ \subset \mathcal{M}$ as the set of links for which agent i is the positive end and $\mathcal{M}_i^- \subset \mathcal{M}$ as the set of links for which node i is the negative end. We define the $N \times M$ *incidence matrix* B as

$$b_{ik} = \begin{cases} +1 & k \in \mathcal{M}_i^+ \\ -1 & k \in \mathcal{M}_i^- \\ 0 & \text{otherwise.} \end{cases} \tag{1}$$

We note that the rank of B is $N-1$ when the graph is connected and that the columns of B are linearly independent when no cycles exist in the graph. Finally, let $\mathbf{1} = [1 \quad \cdots \quad 1]^\top \in \mathbb{R}^N$. It follows from (1) that $B^\top \mathbf{1} = 0$, that is, $\mathbf{1}$ is in the null space of $B^\top$.

B. Attitude kinematics, dynamics, and unit quaternions

The attitude of a rigid body is represented by a 3×3 rotation matrix with positive determinant: an element of $\mathsf{SO}(3)$, the special orthogonal group of order three, defined as

$$\mathsf{SO}(3) = \{R \in \mathbb{R}^{3\times 3} : R^\top R = RR^\top = I, \det R = 1\}.$$

The cross product between two vectors $y, z \in \mathbb{R}^3$, can be written as the matrix multiplication: $y \times z = [y]_\times z$, where

$$[y]_\times = \begin{bmatrix} 0 & -y_3 & y_2 \\ y_3 & 0 & -y_1 \\ -y_2 & y_1 & 0 \end{bmatrix}.$$

The attitude of the ith agent is denoted as R_i, where R_i rotates vectors expressed in body coordinates of the ith agent to their inertial frame coordinates. We let ω_i denote the angular velocity of the ith agent and $J_i = J_i^\top > 0$ is the inertia matrix of the ith agent. When τ_i is a vector of external torques, the kinematic and dynamic equations for each agent are

$$\dot{R}_i = R_i [\omega_i]_\times \tag{2a}$$

$$J_i \dot{\omega}_i = [J_i \omega_i]_\times \omega_i + \tau_i. \tag{2b}$$

A unit quaternion is defined as

$$q = \begin{bmatrix} \eta & \epsilon^\top \end{bmatrix}^\top \in \mathbb{S}^3, \tag{3}$$

where $\mathbb{S}^3 = \{(\eta, \epsilon) \in \mathbb{R} \times \mathbb{R}^3 : \eta^2 + \epsilon^\top \epsilon = 1\}$. A unit quaternion $q \in \mathbb{S}^3$ is mapped to an element of $\mathsf{SO}(3)$ through the Rodrigues formula, $\mathcal{R} : \mathbb{S}^3 \to \mathsf{SO}(3)$, defined as

$$\mathcal{R}(q) = I + 2\eta [\epsilon]_\times + 2 [\epsilon]_\times^2. \tag{4}$$

For convenience in notation, we will often write a quaternion as $q = (\eta, \epsilon)$, rather than in the form of a vector. With the identity element $\mathbf{i} = (1, 0) \in \mathbb{S}^3$, each unit quaternion $q \in \mathbb{S}^3$ has an inverse $q^{-1} = (\eta, -\epsilon)$ under the quaternion multiplication rule

$$q_1 \odot q_2 = \begin{bmatrix} \eta_1\eta_2 - \epsilon_1^\top \epsilon_2 \\ \eta_1\epsilon_2 + \eta_2\epsilon_1 + [\epsilon_1]_\times \epsilon_2 \end{bmatrix},$$

where, for each $i \in \{1, 2\}$, $q_i = (\eta_i, \epsilon_i) \in \mathbb{R} \times \mathbb{R}^3$.

When representing R_i with a unit quaternion q_i, we must "lift" the attitude kinematic equation (2a) onto $\mathbb{S}^3$. In this direction, we define $\nu : \mathbb{R}^3 \to \mathbb{R}^4$ as the map

$$\nu(x) = \begin{bmatrix} 0 & x^\top \end{bmatrix}^\top. \tag{5}$$

Then, the quaternion kinematic equation for agent i satisfies

$$\dot{q}_i = \begin{bmatrix} \dot{\eta}_i \\ \dot{\epsilon}_i \end{bmatrix} = \frac{1}{2} q_i \odot \nu(\omega_i) = \frac{1}{2} \begin{bmatrix} -\epsilon_i^\top \\ \eta_i I + [\epsilon_i]_\times \end{bmatrix} \omega_i. \tag{6}$$

C. Relative attitude error coordinates and synchronization

For every $k \in \mathcal{M}$, we define the relative attitude and angular velocities for each graph link as

$$\tilde{q}_k = q_j^{-1} \odot q_i \qquad \tilde{\omega}_k = \omega_i - \mathcal{R}(\tilde{q}_k)^\top \omega_j \tag{7}$$

where $k \in \mathcal{M}_i^+ \cap \mathcal{M}_j^-$, for $i \neq j$. That is, agent i and agent j are the positive and negative vertex for link k, respectively, and $\tilde{q}_k$ is a relative attitude between them. We group these variables together as

$$\tilde{q} = (\tilde{q}_1, \dots, \tilde{q}_M),\ \tilde{\omega} = (\tilde{\omega}_1, \dots, \tilde{\omega}_M),\ \omega = (\omega_1, \dots, \omega_N). \tag{8}$$

With this definition, it is well known [2]–[4], [15] that the error quaternion $\tilde{q}_k$ satisfies the kinematic equation

$$\dot{\tilde{q}}_k = \frac{1}{2} \tilde{q}_k \odot \nu(\tilde{\omega}_k) \qquad \forall k \in \mathcal{M}. \tag{9}$$

An important property of (7) is that we can express $\tilde{\omega}$ in terms of the $3N \times 3M$ *Rotational Incidence Matrix* $\tilde{B}(\tilde{q})$, which we define in terms of its 3×3 sub-matrices as

$$\tilde{b}_{ik}(\tilde{q}_k) = \begin{cases} I & k \in \mathcal{M}_i^+ \\ -\mathcal{R}(\tilde{q}_k)^\top & k \in \mathcal{M}_i^- \\ 0 & \text{otherwise,} \end{cases} \tag{10}$$

where $i \in \mathcal{N}$ and $k \in \mathcal{M}$. From (7), (8), and (10) we have

$$\tilde{\omega} = \tilde{B}(\tilde{q})^\top \omega. \tag{11}$$

To synchronize the angular rate of each agent to a constant desired angular rate, ω_d, we assume that each agent has access to ω_d. The angular rate error for each agent is defined as

$$\bar{\omega}_i = \omega_i - \omega_d, \tag{12}$$

where $i \in \{1, \dots, N\}$. This definition yields the angular rate error dynamics for each agent as

$$J_i \dot{\bar{\omega}}_i = [J_i \omega_i]_\times \bar{\omega}_i + [J_i \omega_i]_\times \omega_d + \tau_i. \tag{13}$$

For an efficient notation, we define

$$\begin{aligned} \mathscr{J} &= \operatorname{diag}(J_1, \dots, J_N) & \tau &= (\tau_1, \dots, \tau_N) \\ \mathscr{S}(\omega) &= \operatorname{diag}\left([J_1\omega_1]_\times, \dots, [J_N\omega_N]_\times\right) & \bar{\omega} &= (\bar{\omega}_1, \dots, \bar{\omega}_N) \end{aligned}$$

Given $X \in \mathbb{R}^{n\times m}$ and $Y \in \mathbb{R}^{p\times q}$, we let $X \otimes Y$ denote their Kronecker product, defined as the $np \times mq$ matrix

$$X \otimes Y = \begin{bmatrix} x_{11}Y & \cdots & x_{1m}Y \\ \vdots & \ddots & \vdots \\ x_{n1}Y & \cdots & x_{nm}Y \end{bmatrix}.$$

Then, we can write the plant error dynamics as

$$\mathscr{J}\dot{\bar{\omega}} = \mathscr{S}(\omega)\bar{\omega} + \mathscr{S}(\omega)(\mathbf{1} \otimes \omega_d) + \tau, \tag{14}$$

where, recalling (12), $\bar{\omega}$ can be written compactly as

$$\bar{\omega} = \omega - \mathbf{1} \otimes \omega_d. \tag{15}$$

We group the plant error states together and denote their dynamics, given by (9) and (14), as

$$\bar{x}_p = (\tilde{q}, \bar{\omega}) \qquad \dot{\bar{x}}_p = F_p(x_p, \tau). \tag{16}$$

Finally, we let

$$\mathcal{X}_p = \mathbb{S}^{3^N} \times \mathbb{R}^{3N} \qquad x_p = (q, \omega) \in \mathcal{X}_p$$

denote the plant state space and state, respectively. Then, the synchronization objective is to globally and asymptotically stabilize the compact set

$$\mathcal{A}_p = \{x_p \in \mathcal{X}_p : \tilde{q}_k = \pm\mathbf{i}\ \forall k \in \mathcal{M},\ \bar{\omega} = 0\}. \tag{17}$$

D. Hybrid systems framework

A hybrid system is a dynamical system that allows for both continuous and discrete evolution of the state. In this paper, we follow the framework of [17], where a hybrid system $\mathcal{H}$ is defined by four objects: a *flow map*, f, governing continuous evolution of the state by a differential inclusion, a *jump map*, G, governing discrete evolution of the state by a difference inclusion, a *flow set*, C, dictating where flows are allowed, and a *jump set*, D, dictating where jumps are allowed. Given a state $x \in \mathbb{R}^n$, we write a hybrid system in the compact form

$$\mathcal{H}\begin{cases} \dot{x} = f(x) & x \in C \\ x^+ \in G(x) & x \in D. \end{cases}$$

In this paper, the closed-loop system has the flow map continuous, the jump map outer semicontinuous[1]and locally bounded, and the flow and jump sets closed. These properties ensure that asymptotic stability is robust to small perturbations [18]. We refer the reader to [19] for solutions to hybrid systems subjected to disturbances.

III. Robustly Synchronizing Hybrid Controller

A. The hybrid controller

We define a hybrid controller for each agent as follows. Let

$$h = (h_1, \dots, h_M) \in \{-1,1\}^M = \overbrace{\{-1,1\} \times \cdots \times \{-1,1\}}^{M \text{ times}}$$

denote a vector of binary logic variables, where h_k is associated with link $k \in \mathcal{M}$. The controller for the ith agent will define the dynamics for all h_k such that $k \in \mathcal{M}_i^+$. We define the state space and state, respectively, as

$$\mathcal{X} = \mathcal{X}_p \times \{-1,1\}^M \qquad x = (x_p, h) \in \mathcal{X}.$$

The controller utilizes a hysteresis parameter $\delta \in (0,1)$. Then, we define the flow and jump sets for the ith agent as

$$\begin{aligned} C_i &= \{x \in \mathcal{X} : \forall k \in \mathcal{M}_i^+\ h_k\tilde{\eta}_k \geq -\delta\} \\ D_i &= \{x \in \mathcal{X} : \exists k \in \mathcal{M}_i^+\ h_k\tilde{\eta}_k \leq -\delta\}. \end{aligned} \tag{18}$$

We define the set-valued map $\overline{\operatorname{sgn}} : \mathbb{R} \rightrightarrows \{-1,1\}$ as

$$\overline{\operatorname{sgn}}(s) = \begin{cases} s/|s| & s \neq 0 \\ \{-1,1\} & s = 0. \end{cases} \tag{19}$$

Let $\alpha \in [0, \delta)$. The hybrid controller for the ith agent is

$$\forall k \in \mathcal{M}_i^+ \qquad \begin{aligned} \dot{h}_k &= 0 & x &\in C_i \\ h_k^+ &\in h_k\overline{\operatorname{sgn}}(h_k\tilde{\eta}_k + \alpha) & x &\in D_i, \end{aligned} \tag{20a}$$

which takes ω_i, ω_d and $\tilde{q}_k$, $k \in \mathcal{M}_i^+ \cup \mathcal{M}_i^-$ as input and produces the torque output

$$\mathcal{T}_i(x) = -[J_i\omega_i]_\times \omega_d - \sum_{k=1}^{M} b_{ik}h_k\ell_k\tilde{\epsilon}_k - K_i\bar{\omega}_i, \tag{20b}$$

where $\ell_k > 0$ for all $k \in \mathcal{M}$ and $K_i = K_i^\top > 0$ for all $i \in \mathcal{N}$.

B. The closed-loop system

We define flow and jump sets for the network as

$$C = \bigcap_{i=1}^{N} C_i \qquad D = \bigcup_{i=1}^{N} D_i. \tag{21}$$

That is, a jump occurs when at least one agent's controller jumps, but otherwise, the network flows. When there exist $i, j \in \mathcal{N}$, with $i \neq j$ and $x \in D_i \cap D_j$, multiple jumps can occur at the same time instant in no particular order.

Each agent's controller (20) operates on only a subset of the variables in h. We model this as follows. Let $\gamma_{ik} : \mathcal{X} \rightrightarrows \{-1,1\}$ and $\gamma_i : \mathcal{X} \rightrightarrows \{-1,1\}^M$ be defined as

$$\begin{aligned} \gamma_{ik}(x) &= \begin{cases} h_k\overline{\operatorname{sgn}}(h_k\tilde{\eta}_k + \alpha) & k \in \mathcal{M}_i^+ \\ h_k & k \notin \mathcal{M}_i^+ \end{cases} \\ \gamma_i(x) &= \begin{bmatrix} \gamma_{i1}(x) & \cdots & \gamma_{iM}(x) \end{bmatrix}. \end{aligned} \tag{22}$$

[1]A set-valued map $G : X \rightrightarrows Y$ ($\rightrightarrows$ denotes a map to the subsets of the codomain) is outer semicontinuous if for all $x \in X$ and all sequences $x_i \to x$, $y_i \in G(x_i)$ such that $y_i \to y$, we have $y \in G(x)$.

We define a set-valued aggregate jump map as

$$\mathcal{I}(x) = \{i \in \mathcal{N} : x \in D_i\} \qquad \Gamma(x) = \bigcup_{i \in \mathcal{I}(x)} \{\gamma_i(x)\}. \quad (23)$$

We define the aggregate variables

$$\begin{aligned} \mathscr{K} &= \operatorname{diag}(K_1, \ldots, K_N) \quad \tilde{\eta} = (\tilde{\eta}_1, \ldots, \tilde{\eta}_M) \\ H &= \operatorname{diag}(h_1, \ldots, h_M) \quad \tilde{\epsilon} = (\tilde{\epsilon}_1, \ldots, \tilde{\epsilon}_M) \\ \mathscr{L} &= \operatorname{diag}(\ell_1, \ldots, \ell_M). \end{aligned}$$

Then, with the aggregate feedback $\tau = \mathcal{T}(x)$, where

$$\mathcal{T}(x) = \begin{bmatrix} \mathcal{T}_1(x) \\ \vdots \\ \mathcal{T}_N(x) \end{bmatrix} = -\mathscr{S}(\omega)(\mathbf{1} \otimes \omega_d) - (BH\mathscr{L} \otimes I)\tilde{\epsilon} - \mathscr{K}\bar{\omega},$$

with entries defined in (20b), the closed-loop error system is

$$\underbrace{\begin{aligned} \dot{\tilde{q}}_k &= \frac{1}{2}\tilde{q}_k \odot \nu(\tilde{\omega}_k) \quad \forall k \in \mathcal{M} \\ \mathscr{J}\dot{\bar{\omega}} &= \mathscr{S}(\omega)\bar{\omega} - (BH\mathscr{L} \otimes I)\tilde{\epsilon} - \mathscr{K}\bar{\omega} \\ \dot{h} &= 0 \end{aligned}}_{x \in C} \qquad \underbrace{\begin{aligned} \tilde{q}^+ &= \tilde{q} \\ \bar{\omega}^+ &= \bar{\omega} \\ h^+ &\in \Gamma(x) \end{aligned}}_{x \in D}. \quad (24)$$

We denote the flow and jump maps of (24) as

$$F(x) = \begin{bmatrix} F_p(x_p, \mathcal{T}(x)) \\ 0 \end{bmatrix} \quad G(x) = \begin{bmatrix} \{\bar{x}_p\} \\ \Gamma(x) \end{bmatrix}$$

and condense (24) into the compact form

$$\bar{x} = (\bar{x}_p, h) \qquad \begin{aligned} \dot{\bar{x}} &= F(x) \quad x \in C \\ \bar{x}^+ &\in G(x) \quad x \in D. \end{aligned}$$

Before proceeding to the main results, we slightly generalize [3, Lemma 2] by introducing a diagonal matrix.

Lemma 1. *For any diagonal matrix*

$$\mathscr{D} = \operatorname{diag}(d_1, \ldots, d_M),$$

the rotational incidence matrix satisfies

$$\tilde{B}(\tilde{q})(\mathscr{D} \otimes I)\tilde{\epsilon} = (B\mathscr{D} \otimes I)\tilde{\epsilon}, \quad (25)$$

where $\tilde{B}$ is as defined in (10)*.*

Proof: Let $\tilde{B}_i(\tilde{q}) = \begin{bmatrix} \tilde{b}_{i1} & \cdots & \tilde{b}_{iM} \end{bmatrix}$. Expanding the left-hand side of (25) by means of (10), we see that

$$\tilde{B}_i(\tilde{q})(\mathscr{D} \otimes I)\tilde{\epsilon} = \sum_{k \in \mathcal{M}_i^+} d_k \tilde{\epsilon}_k - \sum_{p \in \mathcal{M}_i^-} \mathcal{R}(\tilde{q}_p)^\top d_p \tilde{\epsilon}_p. \quad (26)$$

Now, applying the fact that $\mathcal{R}(\tilde{q}_p)^\top \epsilon_p = \epsilon_p$, it follows from (1) and matching terms in (26) that

$$\sum_{k \in \mathcal{M}_i^+} d_k \tilde{\epsilon}_k - \sum_{p \in \mathcal{M}_i^-} \mathcal{R}(\tilde{q}_p)^\top d_p \tilde{\epsilon}_p = \sum_{k=1}^{M} b_{ik} d_k \tilde{\epsilon}_k$$

so that for every $i \in \mathcal{N}$, $\tilde{B}_i(\tilde{q})(\mathscr{D} \otimes I)\tilde{\epsilon} = (B_i \mathscr{D} \otimes I)\tilde{\epsilon}$, where $B_i = \begin{bmatrix} b_{i1} & \cdots & b_{iM} \end{bmatrix}$. This proves the result. ■

We can now prove stability of the compact set

$$\mathcal{A} = \{x \in \mathcal{X} : \tilde{q} = H\mathbf{1} \otimes \mathbf{i},\ \bar{\omega} = 0\}$$

and global attractivity of the set

$$\mathcal{E} = \{x \in C : (BH\mathscr{L} \otimes I)\tilde{\epsilon} = 0,\ \bar{\omega} = 0\}.$$

First we note that if the graph is connected and acyclic, $\mathcal{E} = \mathcal{A}$.

Lemma 2. *If $0 < \delta < 1$, $\ell_k > 0$ for all $k \in \mathcal{M}$, and B is connected and acyclic, then, $\mathcal{E} = \mathcal{A}$.*

Proof: If B is connected and acyclic, then it has full column rank. Then, since $\ell_k > 0$ for all $k \in \mathcal{M}$, it follows that $(BH\mathscr{L} \otimes I)\tilde{\epsilon} = 0$ implies that $\tilde{\epsilon} = 0$ and $|\tilde{\eta}_k| = 1$ for all $k \in \mathcal{M}$. If $x \in C$, then for all $k \in \mathcal{M}$, it follows that $h_k\tilde{\eta}_k \geq -\delta > -1$. Finally, since $h_k \in \{-1, 1\}$, it follows that $h_k\tilde{\eta}_k = 1$ for all $k \in \mathcal{M}$. This means that $\tilde{q}_k = (\tilde{\eta}_k, \tilde{\epsilon}_k) = (h_k, 0) = h_k\mathbf{i}$ for all $k \in \mathcal{M}$, or equivalently, $\tilde{q} = H\mathbf{1} \otimes \mathbf{i}$. ■

Theorem 3. *Suppose that $0 \leq \alpha < \delta < 1$, $\ell_k > 0$ for all $k \in \mathcal{M}$, and $K_i = K_i^\top > 0$ for all $i \in \mathcal{N}$. Then, the compact set $\mathcal{A}$ is stable and the compact set $\mathcal{E} \supset \mathcal{A}$ is globally attractive for the closed-loop hybrid system defined by* (6)*,* (2b)*,* (20a)*,* (20b)*, with error dynamics* (24)*. When B is connected and acyclic, $\mathcal{A} = \mathcal{E}$ so that $\mathcal{A}$ is globally asymptotically stable.*

Proof: Consider the Lyapunov function

$$V(x) = 2\mathbf{1}^\top \mathscr{L}(\mathbf{1} - H\tilde{\eta}) + \tfrac{1}{2}\bar{\omega}^\top \mathscr{J}\bar{\omega}.$$

Since $\ell_k > 0$ for all $k \in \mathcal{M}$ and $J_i = J_i^\top > 0$ for all $i \in \mathcal{N}$, $V(x) > 0$ for all $x \in \mathcal{X} \setminus \mathcal{A}$ and $V(x) = 0$ for all $x \in \mathcal{A}$. We now examine the evolution of V along solutions of (24).

First, we calculate the change in V along flows as

$$\begin{aligned} \langle \nabla V(x), F(x) \rangle &= \tilde{\omega}^\top (H\mathscr{L} \otimes I)\tilde{\epsilon} \\ &\quad + \bar{\omega}^\top \left(\mathscr{S}(\omega)\bar{\omega} - (BH\mathscr{L} \otimes I)\tilde{\epsilon} - \mathscr{K}\bar{\omega}\right). \end{aligned}$$

Recalling from (11) that $\tilde{\omega} = \tilde{B}^\top(\tilde{q})\omega$ and noting that $H\mathscr{L}$ is diagonal, we apply Lemma 1 and see that

$$\tilde{\omega}^\top (H\mathscr{L} \otimes I)\tilde{\epsilon} = \omega^\top \tilde{B}(\tilde{q})(H\mathscr{L} \otimes I)\tilde{\epsilon} = \omega^\top (BH\mathscr{L} \otimes I)\tilde{\epsilon}.$$

Then, noting that $\mathscr{S}^\top(\omega) = -\mathscr{S}(\omega)$, it follows that $\bar{\omega}^\top \mathscr{S}(\omega)\bar{\omega} = 0$, and

$$\begin{aligned} \langle \nabla V(x), F(x) \rangle &= -\bar{\omega}^\top \mathscr{K}\bar{\omega} + \omega^\top (BH\mathscr{L} \otimes I)\tilde{\epsilon} \\ &\quad - (\omega - \mathbf{1} \otimes \omega_d)^\top (BH\mathscr{L} \otimes I)\tilde{\epsilon}. \end{aligned}$$

Finally, applying the property that

$$(\mathbf{1} \otimes \omega_d)^\top (BH\mathscr{L} \otimes I) = (\mathbf{1}^\top BH\mathscr{L} \otimes \omega_d),$$

and recalling that $\mathbf{1}^\top B = 0$, it follows that

$$\langle \nabla V(x), F(x) \rangle = -\bar{\omega}^\top \mathscr{K}\bar{\omega}.$$

Since $K_i = K_i^\top > 0$ for all $i \in \mathcal{N}$, $\langle \nabla V(x), F(x) \rangle \leq 0$ for all $x \in C \setminus \mathcal{A}$ and so V is nonincreasing along flows.

Examining V over jumps, we see that for all $g \in G(x)$,

$$V(g) - V(x) \in \bigcup_{i \in \mathcal{I}(x)} \left\{ 2\sum_{k=1}^{M} \ell_k (h_k - \gamma_{ik}(x))\tilde{\eta}_k \right\},$$

where $\mathcal{I}(x)$ was defined in (23). Then, since

$$\sum_{k=1}^{M} \ell_k (h_k - \gamma_{ik}(x))\tilde{\eta}_k = \sum_{k \in \mathcal{M}_i^+} \ell_k h_k \tilde{\eta}_k (1 - \overline{\operatorname{sgn}}(h_k\tilde{\eta}_k + \alpha))$$

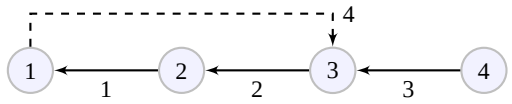

Fig. 1. Serial network with four agents. Addition of fourth link makes a three-agent cycle.

and for $i \in \mathcal{I}(x)$, there exists $k \in \mathcal{M}_i^+$ such that $h_k \tilde{\eta}_k \leq -\delta$, it follows that

$$\max_{w \in G(x)} V(w) - V(x) \leq -4\ell_k \delta \leq -4\delta \min_{k \in \mathcal{M}} \ell_k < 0$$

so that $\max_{w \in G(x)} V(w) - V(x) < 0$ for all $x \in D$. It follows from [20, Theorem 7.6] that $\mathcal{A}$ is stable.

Applying an invariance principle for hybrid systems, [20, Theorem 4.7], we see that closed-loop trajectories approach the largest weakly invariant set contained in

$$W = \{x \in C : \langle \nabla V(x), F(x) \rangle = 0\} = \{x \in C : \bar{\omega} = 0\}.$$

Since holding $\bar{\omega} \equiv 0$ implies that $\dot{\bar{\omega}} = 0$, it follows from (24) that x must converge to $\mathcal{E} = \{x \in C : (BH\mathscr{L} \otimes I)\tilde{\epsilon} = 0,\ \bar{\omega} = 0\}$. The result then follows from Lemma 2. ■

We assert the robustness of stability to measurement and actuation disturbances in terms of a $\mathcal{KL}$ estimate. The following result is a direct consequence of [18, Theorem 6.6] and the fact that the closed-loop system satisfies the hybrid basic conditions [17, A1-A3]. In what follows, $\sigma\mathbb{B} = \{x \in \mathbb{R}^n : |x| \leq \sigma\}$ (n is determined by context) and $|x|_{\mathcal{A}} = \inf\{|x - y| : y \in \mathcal{A}\}$.

Theorem 4. *Under all assumptions of Theorem 3, there exists a class-$\mathcal{KL}$ function $\beta : \mathbb{R}_{\geq 0} \times \mathbb{R}_{\geq 0} \to \mathbb{R}_{\geq 0}$ such that for each $\gamma > 0$ and each compact set $\mathcal{K} \subset \mathbb{R}^{3N}$ there exists $\sigma > 0$ such that each solution (x_p, h, e) to the closed-loop system defined by* (6), (2b), (20a), (20b), *and $\tau = \mathcal{T}(x_p + e, h)$, with error dynamics satisfying*

$$\underbrace{\begin{aligned} \dot{\bar{x}}_p &= F_p(x_p, \mathcal{T}(x_p + e, h)) \\ \dot{h} &= 0 \end{aligned}}_{(x_p + e, h) \in C} \qquad \underbrace{\begin{aligned} \bar{x}_p^+ &= \bar{x}_p \\ h^+ &\in \Gamma(x_p + e, h) \end{aligned}}_{(x_p + e, h) \in D},$$

$e : \operatorname{dom} e \to \sigma\mathbb{B}$ measurable, and $x(0,0) \in \mathbb{S}^{3^N} \times \mathcal{K} \times \{-1, 1\}^M$ satisfies

$$|x(t,j)|_{\mathcal{A}} \leq \beta\left(|x(0,0)|_{\mathcal{A}}, t + j\right) + \gamma \qquad \forall (t,j) \in \operatorname{dom} x.$$

IV. Simulation Study

In this simulation study, we consider a network of four identical agents where $J_i = \operatorname{diag}(4.35, 4.33, 3.664)$ (as in [1]) and $K_i = I$ for $i = 1, 2, 3, 4$. In each simulation, $\omega_d = 0$. For each $k \in \mathcal{M}$, $l_k = 1$. The initial angular velocities, $\omega_i(0)$, and the initial attitude errors, $\tilde{q}_k$ are specified on a per-simulation basis later in the section; however, $h_k(0) = 1$ for all $k \in \mathcal{M}$. The network is shown in Fig. 1; whether or not link 4 is enabled is specified on a per-simulation basis. All simulations were conducted in MATLAB/Simulink using a fixed-step solver with step size of $1/100$s. The unit-quaternion states q_i were first normalized before subsequent calculations.

For each simulation, we provide plots depicting relative attitude errors and jumps of the hybrid controller. The $h_k \tilde{\eta}_k$ plot shows, for each link, the logic variable h_k multiplied by $\tilde{\eta}_k$. Discontinuities in this plot occur when h_k changes its sign over a jump. The $\theta(\tilde{q}_k)$ plot shows, for each link, the error angle between two agents across a link. For some quaternion $q = (\eta, \epsilon)$, its angle from $\pm\mathbf{i}$ is defined as $\theta(q) = 2\cos^{-1}(|\eta|)$. Due to space constraints, angular velocity errors are not shown.

The simulations in Figs. 2, 3, and 4 were conducted with four agents having initial conditions

$$\begin{bmatrix} q_1^\top(0) \\ q_2^\top(0) \\ q_3^\top(0) \\ q_4^\top(0) \end{bmatrix} = \frac{1}{\sqrt{2}} \begin{bmatrix} 1 & 1 & 0 & 0 \\ -1 & 1 & 0 & 0 \\ 1 & 0 & 1 & 0 \\ 1 & 0 & 1 & 0 \end{bmatrix} \tag{27}$$

$$\begin{bmatrix} \omega_1^\top(0) \\ \omega_2^\top(0) \\ \omega_3^\top(0) \\ \omega_4^\top(0) \end{bmatrix} = \frac{9}{10} \begin{bmatrix} 1 & 1 & -1 \\ 2 & -2 & 2 \\ 1 & -1 & -1 \\ -1 & 1 & 1 \end{bmatrix} \tag{28}$$

The simulations in Figs. 2 and 4 were conducted with the serial graph structure pictured in Fig. 1 (i.e. *without* the dashed link 4). The simulation in Fig. 3 was conducted with the cyclic graph structure illustrated in Fig. 1 (i.e. *with* the dashed link 4). With this graph, the initial relative attitude errors are

$$\begin{bmatrix} \tilde{q}_1^\top(0) \\ \tilde{q}_2^\top(0) \\ \tilde{q}_3^\top(0) \\ \tilde{q}_4^\top(0) \end{bmatrix} = \begin{bmatrix} 0 & -1 & 0 & 0 \\ -1/2 & 1/2 & 1/2 & 1/2 \\ 1 & 0 & 0 & 0 \\ -1/2 & 1/2 & -1/2 & -1/2 \end{bmatrix}. \tag{29}$$

The simulations in Figs. 2 and 3 illustrate the efficacy of the proposed hybrid scheme and show how synchronization can be compromised by cycles within the graph. From the initial condition described above, the proposed hybrid scheme synchronizes the attitude of each agent when the graph is connected and acyclic, as depicted in Fig 2. The introduction of the 4th (dashed) link from agent 1 to 3 in Fig. 1 destroys this global synchronization property. As shown in Fig. 3, only one relative error angle corresponding to the link outside of the cycle converges to zero. As discussed in [3], the three agents in the cycle (agents 1,2, and 3) settle into a configuration where $\sum_{k=1}^{3} \theta(\tilde{q}_k) = 2\pi$. Both simulations have $\delta = 0.45$.

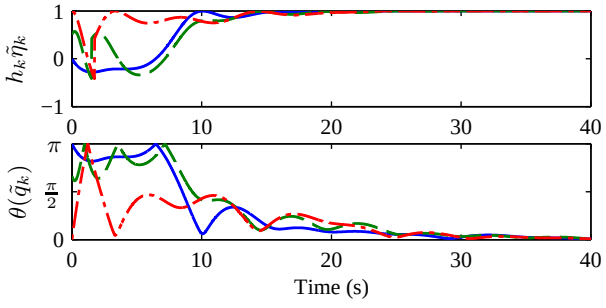

Fig. 2. Synchronization with hybrid controller on serial network.

To illustrate how the hybrid scheme avoids unwinding with $\delta \in (0, 1)$, we repeated the simulation of Fig. 2 (the serial, connected, and acyclic network) with one crucial change: we set $\delta = 2$. This change disables switching of any h_k, since

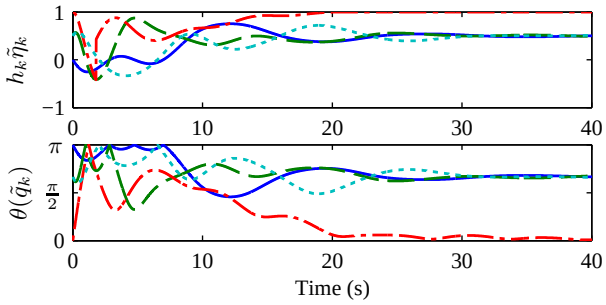

Fig. 3. Convergence to non-synchronized state on cyclic network.

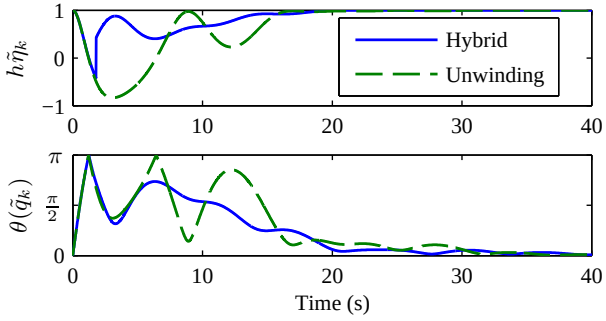

Fig. 4. Link that exhibits unwinding after disabling hysteretic jumps.

$\tilde{\eta}_k h_k \leq -\delta$ can never be satisfied. Then, for each $k \in \mathcal{M}$, $\tilde{q}_k$ is driven towards $h_k(0)\mathbf{i} = \mathbf{i}$. Fig. 4 shows the two situations in parallel: the plot labeled "Hybrid" shows $h_k\tilde{\eta}_k$ and $\theta(\tilde{q}_k)$ from Fig. 2, while the plot labeled "Unwinding" shows the same values when $\delta = 2$, with the same initial conditions and parameters, other than δ. Note that $h_k\tilde{\eta}_k = \tilde{\eta}_k$ for the "Unwinding" plot, since $h_k(0) = 1$ and h_k cannot switch during the simulation. Fig. 4 shows that the unwinding-inducing controller causes large angular oscillations in the response as it forces $\tilde{q}_3$ towards $\mathbf{i}$. In this case, the relative angle between the agents increases from zero to $\pi/2$ in approximately 2s and continues to rotate. The hybrid controller with $\delta = 0.45$ switches the value of h_k as $h_k\tilde{\eta}_k$ passes $-\delta$. In contrast, the unwinding-inducing controller remains set on forcing $\tilde{q}_3$ to $\mathbf{i}$, despite the fact that $\tilde{q}_3$ is closer to $-\mathbf{i}$.

V. Conclusion

Existing attitude-synchronization schemes fall victim to topological difficulties: any continuous control will fail to be globally asymptotically stabilizing [11] and discontinuous quaternion-based state-feedback control laws are not robust to measurement disturbances [15]. To solve these issues, we employed a hybrid control law that utilizes a single binary logic variable associated with each relative attitude error that hysteretically switches the sign of a torque component applied by neighboring agents. For connected and acyclic graphs, the result is a robust global asymptotic synchronization scheme that manages a trade-off between unwinding and robustness to measurement disturbances through the hysteresis width. While we have treated the case when the desired angular velocity is constant, it is possible to extend the results to the time-varying case using a similar procedure to [15]. The control law proposed in this note depends upon knowledge of the inertia matrix and it may be possible to eliminate this dependence by the addition of adaptive mechanisms (e.g. [21]). Finally, the synchronization scheme presented in this note requires that neighboring agents can communicate logic variables and have have a consistent quaternion representation of their relative attitude error. It may be possible to relax these restrictions; however, this is topic for future research.

References

[1] R. Kristiansen, A. Loría, A. Chaillet, and P. J. Nicklasson, "Spacecraft relative rotation tracking without angular velocity measurements," *Automatica*, vol. 45, no. 3, pp. 750–756, Mar. 2009.

[2] A. Abdessameud and A. Tayebi, "Attitude synchronization of a group of spacecraft without velocity measurements," *IEEE Transactions on Automatic Control*, vol. 54, no. 11, pp. 2642–2648, Oct. 2009.

[3] H. Bai, M. Arcak, and J. T. Wen, "Rigid body attitude coordination without inertial frame information," *Automatica*, vol. 44, no. 12, pp. 3170–3175, Dec. 2008.

[4] J. R. Lawton and R. W. Beard, "Synchronized multiple spacecraft rotations," *Automatica*, vol. 38, no. 8, pp. 1359–1364, Aug. 2002.

[5] J. Erdong and S. Zhaowei, "Robust attitude synchronisation controllers design for spacecraft formation," *IET Control Theory & Applications*, vol. 3, no. 3, pp. 325–339, Mar. 2009.

[6] D. V. Dimarogonas, P. Tsiotras, and K. J. Kyriakopoulos, "Leader-follower cooperative attitude control of multiple rigid bodies," *Systems & Control Letters*, vol. 58, no. 6, pp. 429–435, Jun. 2009.

[7] A. Sarlette, R. Sepulchre, and N. E. Leonard, "Autonomous rigid body attitude synchronization," *Automatica*, vol. 45, no. 2, pp. 572–577, Feb. 2009.

[8] T. Krogstad and J. Gravdahl, "Coordinated attitude control of satellites in formation," in *Group Coordination and Cooperative Control*, ser. Lecture Notes in Control and Information Sciences. Springer, 2006, ch. 9, pp. 153–170.

[9] K. Lau, S. Lichten, L. Young, and B. Haines, "An innovative deep space application of GPS technology for formation flying spacecraft," in *AIAA Guidance, Navigation, and Control Conference*, 1996, paper no. AIAA-96-3819.

[10] J. P. How, R. Twiggs, D. Weidow, K. Hartman, and F. Bauer, "Orion: A low-cost demonstration of formation flying in space using GPS," in *AIAA/AAS Astrodynamics Specialist Conference and Exhibit*, 1998, paper no. AIAA-1998-4398.

[11] S. P. Bhat and D. S. Bernstein, "A topological obstruction to continuous global stabilization of rotational motion and the unwinding phenomenon," *Systems & Control Letters*, vol. 39, no. 1, pp. 63–70, Jan. 2000.

[12] N. A. Chaturvedi, N. H. McClamroch, and D. S. Bernstein, "Asymptotic smooth stabilization of the inverted 3-D pendulum," *IEEE Transactions on Automatic Control*, vol. 54, no. 6, pp. 1204–1215, 2009.

[13] J. Stuelpnagel, "On the parametrization of the three-dimensional rotation group," *SIAM Review*, vol. 6, no. 4, pp. 422–430, Oct. 1964.

[14] C. G. Mayhew, R. G. Sanfelice, and A. R. Teel, "On quaternion-based attitude control and the unwinding phenomenon," in *Proceedings of the American Control Conference*, 2011, pp. 299–304.

[15] ——, "Quaternion-based hybrid control for robust global attitude tracking," *IEEE Transactions on Automatic Control*, 2011, to appear.

[16] M. Arcak, "Passivity as a design tool for group coordination," *IEEE Transactions on Automatic Control*, vol. 52, no. 8, pp. 1380–1390, Aug. 2007.

[17] R. Goebel, R. G. Sanfelice, and A. R. Teel, "Hybrid dynamical systems," *IEEE Control Systems*, vol. 29, no. 2, pp. 28–93, Apr. 2009.

[18] R. Goebel and A. Teel, "Solutions to hybrid inclusions via set and graphical convergence with stability theory applications," *Automatica*, vol. 42, no. 4, pp. 573–587, Apr. 2006.

[19] R. G. Sanfelice, R. Goebel, and A. R. Teel, "Generalized solutions to hybrid dynamical systems," *ESIAM: Control, Optimisation, and Calculus of Variations*, vol. 14, no. 4, pp. 699–724, 2008.

[20] ——, "Invariance principles for hybrid systems with connections to detectability and asymptotic stability," *IEEE Transactions on Automatic Control*, vol. 52, no. 12, pp. 2282–2297, Dec. 2007.

[21] A. Sanyal, A. Fosbury, N. A. Chaturvedi, and D. S. Bernstein, "Inertia-free spacecraft attitude tracking with disturbance rejection and almost global stabilization," *Journal of Guidance, Control, and Dynamics*, vol. 32, no. 4, pp. 1167–1178, 2009.